Dynamical adiabatic theory of atomic collisions: The structure of hidden, avoided, and L_3 crossings

T. P. Grozdanov*
Institute of Physics, University of Belgrade, Pregrevica 118, 11080 Belgrade, Serbia

E. A. Solov'ev
Bogoliubov Laboratory of Theoretical Physics, Joint Institute for Nuclear Research, 141980 Dubna, Moscow region, Russia
(Received 18 June 2014; published 5 September 2014)

Inelastic transitions in slow ion-atom collisions are described using an adiabatic representation of the collision system, where the transition probabilities are determined by the branch points of the potential energy curves in the complex plane of internuclear separation R. As an example, the HeH^{2+} system is treated, in which the evolution of the branch points related to hidden, avoided, and L_3 crossings in the dynamical adiabatic basis of three-body Coulomb problem as functions of parameter $\omega = \rho v$ (ρ is the impact parameter and v the impact velocity) is studied. Rearrangement of hidden couplings due to the passage of L_3 branch points with the increase of ω is discussed.

DOI: 10.1103/PhysRevA.90.032706 PACS number(s): 34.10.+x, 34.20.−b

I. INTRODUCTION

The slow atomic collisions are considered to be those which cover the range of impact energies of up to about 10 keV/nucleon. They are of great importance for description and understanding of a variety of elementary processes occurring in laboratory, fusion, and astrophysical plasmas. The natural choice of theoretical approach in describing these kinds of collisions is the adiabatic approximation, where the collision dynamics is determined by the properties of the quasimolecule formed during the collision.

However, when using an expansion of the wave function in terms of adiabatic eigenstates of the quasimolecule, the problem of obeying the proper boundary conditions occurs because the electrons are asymptotically attached to moving centers (for a review, see [1]). In the quantum description of the motion of the nuclei, the problem is resolved within the hyperspherical adiabatic approach, proposed by Macek [2] for solving the three-body Coulomb problem. The method has been widely applied to variety of collision problems, in particular to the He^{2+} + H system [3] which we shall treat as an example in this work.

On the other hand, in the impact-parameter formulation of the theory (that is, when the motion of the nuclei is described classically), in order to obtain a Galilean invariant theory, it is necessary to attach to each of the basis functions the so-called electron translation factors [1]. An alternative solution to this problem is the method of *nonstationary scaling of length* (NSSL), proposed originally by one of the authors [4]. [We note that the NSSL has also been successfully used to treat the problems of electron-atom (molecule) collisions [5] and the interaction of atoms and molecules with radiation fields [6,7].] The NSSL transformation resolves the principal problem of incompatibility of standard adiabatic basis with the physical boundary conditions [8] [see also Eq. (8) in [9]]. When the standard adiabatic basis is used, it leads sometimes to nonvanishing oscillations of the population of adiabatic states in the limit of internuclear separations $R \to \infty$, so that transition probability cannot be defined. With NSSL, the ion-atom collision problem is reduced to the one in which the nuclei are at rest, but their charges are time dependent and additional dynamical interactions appear in the electronic Hamiltonian [8]. In our recent work [9], we have studied in detail the properties of the resulting *dynamical adiabatic potential energy curves* (DAPEC) as functions of the (real) internuclear separation R. However, for the determination of the transition probabilities in the system, of crucial importance are the crossings (branch points) of analytic continuations of DAPEC into the complex R plane and these are the subject of our present work. We first review below the role of the so-called hidden and narrow avoided crossings in the standard adiabatic approach.

The hidden crossings of electronic adiabatic eigenvalues [*potential energy curves* (PEC)] play a key role in the standard (separable) one-electron two-Coulomb-center problem (see review papers [8,10]). They are present whenever one of the PEC crosses the top of the barrier in the effective electron potential along one of the separable coordinates. Here, according to semiclassical considerations, adiabatic eigenstate $|i\rangle$ dramatically concentrates on the top of barrier involving neighboring state $|f\rangle$ to save smooth behavior of the two-state subspace when the quasimolecule passes this point. As a result, intense transitions between corresponding adiabatic states occur. Hidden crossings cannot be identified on the plot of the PEC for real internuclear separations R. That is why the denotation *hidden crossing* was introduced. But, they are clearly manifested in the matrix element of nonadiabatic coupling $W_{if} = \langle i|d/dR|f\rangle$ which has a maximum at this point. This maximum reflects the presence of a branch point R_b connecting PEC $\varepsilon_i(R)$ and $\varepsilon_f(R)$ of the same symmetry: $\Delta\varepsilon_{if}(R) \sim \sqrt{R - R_b}$. The square-root singularity is due to the fact that in the complex R plane the Hamiltonian is no longer self-adjoint, and, at the point of degeneracy of two eigenvalues $[\varepsilon_i(R_b) = \varepsilon_f(R_b)]$, the Hamiltonian reduces not to a diagonal form but rather to the Jordan form (having nonzero elements on the diagonal and superdiagonal). As a result, in the vicinity of R_b, instead of the usual linear dependence of $\Delta\varepsilon_{if}(R)$ on $R - R_b$ at real R, we have now a square-root dependence. In fact, $\varepsilon_i(R)$ and $\varepsilon_f(R)$ are different

*tasko@ipb.ac.rs

branches of a single (multivalued) analytic function $\varepsilon(R)$. If we adopt the impact-parameter method for the description of a collision problem, that is, assuming the nuclei to follow classical trajectories defined by a given function $R = R(t,\rho,v)$ of time t, impact parameter ρ, and asymptotic relative collision velocity v, then the "single-pass" electron transition probability via the hidden crossing is obtained as an analytic continuation of a time-dependent phase factor of wave function [see, for example, Eq. (8)] along the contour L in the complex R plane which starts at any real R_1 where $\varepsilon(R_1) = \varepsilon_i(R_1)$ goes around a complex branch point R_b and ends up back on any real R_2 where $\varepsilon(R_2) = \varepsilon_f(R_2)$:

$$p_{if}(\rho,v) = \exp\left(-\frac{2}{\hbar}\left|\mathrm{Im}\int_L \varepsilon(R)\frac{dR}{v_R(R,\rho,v)}\right|\right), \qquad (1)$$

where $v_R(R,\rho,v) = dR/dt$ is the radial collision velocity. As analytic estimates show (see Ref. [10], p. 165), for hidden crossings the distance from the real R axis to the branch point R_b is given by an expression which is proportional to the square of the Planck constant $\hbar^2$.

For electronic adiabatic energies below the top of the barrier separating two Coulomb wells, narrow avoided crossings can exist which are due to the resonant underbarrier interaction of two adiabatic states having similar energies and located on the different nuclei. In this case, the analytic estimates (see Ref. [10], p. 165) show that the distance from the real axis to the branch point R_b is given by an expression exponentially small with respect to the inverse of the Planck constant $\hbar$, that is, it is proportional to $\exp(-S/\hbar)$, where S is the modulus of the underbarrier action. The avoided crossings are well pronounced at real R. Here, instead of the quasimolecular (adiabatic) basis, we can use with good accuracy an atomic (diabatic) basis. The transition probability (1) can then be expressed in terms of diabatic potential curves [11]

$$p_{if}(\rho,v) = \exp\left(-\frac{2\pi W_{if}^2(R_c)}{\hbar v_R(R_c,\rho,v)[|F_i(R_c) - F_f(R_c)|]}\right), \qquad (2)$$

where $W_{if}(R)$ is the interaction matrix element of two diabatic states, while $F_i(R)$ and $F_f(R)$ are the slopes of the diabatic PEC with all quantities taken at the (real) point $R = R_c$ of the exact crossing of the diabatic PEC.

Aside from inelastic transitions, which take place via hidden and avoided crossings, there are transitions due to the rotation of the internuclear axis. These transitions are, however, known to be localized in the regions of degeneracies (exact crossings) of the PEC corresponding to states with different symmetries (projections of the electron angular momentum onto the internuclear axis should differ by $\hbar$). Typical regions (aside from the isolated exact crossings) where rotational transitions occur are the united-atom ($R \to 0$) and separated-atom ($R \to \infty$) limits, due to the degeneracies of the corresponding atomic states. In the united-atom limit, rotational transitions take place between states of the same angular quantum number l. For these transitions, the adiabatic approximation has been developed for $l = 1$,

$$p_{if}(\rho,v) = 2\exp\left(-\frac{2}{\hbar}\left|\mathrm{Im}\int_0^{i\rho/v}\Delta\varepsilon_{if}(R(t))dt\right|\right)$$
$$\approx 2\exp\left(-\frac{4}{3v}\alpha_1\rho^3\right), \qquad (3)$$

and for $l = 2$,

$$p_{if}(\rho,v) = 4\exp\left(-\frac{2}{\hbar}\left|\mathrm{Im}\int_0^{i\rho/v}\Delta\varepsilon_{if}(R(t))dt\right|\right)$$
$$\approx 4\exp\left(-\frac{4}{3v}\alpha_2|m_i^2 - m_f^2|\rho^3\right), \qquad (4)$$

where $\Delta\varepsilon_{if}(R) \approx \alpha_l(m_i^2 - m_f^2)R^2$ ($R^2 = \rho^2 + v^2t^2$), m_i and m_f are projections of the electron angular momentum of initial and final states onto the internuclear axis (for details, see review paper [8]). However, for $l = 2$, the adiabatic asymptote (4) is in agreement with the numerical result only at extremely small angular velocity (see Fig. 1 in [12]), and correct probabilities for $l \geqslant 2$ can be obtained only by numerical close-coupling calculations. In the separated-atom limit, the contribution of rotational transitions is reduced to a modification of the correlation diagram [13] which coincides with the correlation diagram in the dynamical adiabatic basis. The rotational transitions due to isolated exact crossings at finite distant R are described by Eq. (2) with the replacement of diabatic PEC by adiabatic PEC.

In the dynamical adiabatic theory, which we started to develop in Ref. [9], the eigenvalue problem for DAPEC is not separable. The only symmetry which we have in this case is the parity $\Pi_3 = \pm 1$ with respect to the reflection $q_3 \to -q_3$ in the modified electron coordinates $\mathbf{q}$, where the $\hat{\mathbf{q}}_3$ axis is directed perpendicular to the scattering plane. In this representation, the rotational transitions are transformed into radial transitions through the component of the angular momentum operator L_3 which now explicitly appears in the Hamiltonian, and a large number of the exact crossings between the states of different symmetry in the two-Coulomb-center basis transform into a type of branch points which we call L_3 crossings. The transition probability related to any type of branch point is determined by an expression similar to Eq. (1), but instead of PEC $\varepsilon(R)$ the DAPEC $E(R,\omega)$ appear, where in the case of straight-line ionic trajectories, the DAPEC depend on a single additional (dynamical) parameter $\omega = \rho v$. In this paper, we shall study the evolution of the hidden, avoided, and L_3 crossings of DAPEC with the change of the parameter ω.

The plan of the article is as follows. In Sec. II, we present the formulation of the problem. Section III contains the description of the numerical method used in the computation of the complex DAPEC and search for the branch points. In Sec. IV, we present the results of the calculation of the ω dependence of a number of branch points of interest for low-energy collisions in the HeH^{2+} system. Concluding remarks are given in Sec. V. Hereafter, we use atomic units except unless explicitly stated.

II. FORMULATION OF THE PROBLEM

We consider a collision system consisting of a single electron and two bare nuclei of charges Z_A and Z_B traveling along the straight-line trajectories in the (x,y)-scattering plane, so that $\mathbf{R}(t) = \mathbf{R}_B(t) - \mathbf{R}_A(t) = vt\hat{\mathbf{x}} + \rho\hat{\mathbf{y}}$. We next modify the electronic time-dependent Schrödinger equation by a series of transformations (for details, see Ref. [9]):

(i) The electronic coordinates (x,y,z) are divided by the internuclear separation $R(t)$ (this corresponds to NSSL) and subsequently transformed to the rotating (molecular)

coordinate system (q_1,q_2,q_3) with the q_1 axis directed along the internuclear axis.

(ii) A suitable overall phase factor is factorized from the total time-dependent wave function in order to obey the correct scattering boundary conditions.

(iii) A "timelike" variable τ is introduced via the relation $d\tau = dt/R(t)^2$. In our case of the straight-line trajectories, one finds $\tau(t) = \omega^{-1}\arctan(vt/\rho)$ with $\omega = \rho v$, so that the variation of t in the interval $(-\infty, +\infty)$ corresponds to the variation of τ in the interval $(\tau_i,\tau_f) \equiv (-\pi/(2\omega), +\pi/(2\omega))$. [We note that there is a misprint in Eq. (7) of Ref. [9] where the prefactor ω should be replaced with ω^{-1}.]

The modified Schrödinger equation for the electron wave function $f(\mathbf{q},\tau)$ is obtained in the form

$$H(\tau)f(\mathbf{q},\tau) = i\frac{\partial f(\mathbf{q},\tau)}{\partial\tau}, \tag{5}$$

with

$$H(\tau) = -\frac{1}{2}\Delta_q - R(\tau)\left(\frac{Z_A}{|\mathbf{q}+\alpha\hat{\mathbf{q}}_1|} + \frac{Z_B}{|\mathbf{q}-\beta\hat{\mathbf{q}}_1|}\right) + \omega L_3 + \frac{1}{2}\omega^2 q^2, \tag{6}$$

where $R(\tau) = \rho/\cos\omega\tau$, $\hat{\mathbf{q}}_1$ is the unit vector along the q_1 axis, α and β ($\alpha+\beta=1$) define the position of the coordinate origin on the internuclear axes, and

$$L_3 = -i\left(q_1\frac{\partial}{\partial q_2} - q_2\frac{\partial}{\partial q_1}\right) \tag{7}$$

is the operator of the projection of the electronic angular momentum onto the direction perpendicular to the scattering plane. L_3 is invariant to the $\mathbf{r}\to\mathbf{q}$ transformation. In the $(\mathbf{q},\tau)$ "representation," the two Coulomb centers are at "rest" and separated by the unit distance, but their strengths are $R(\tau)$ dependent. The Hamiltonian $H(\tau)$ is an even function of τ and the parity $\Pi_3(q_3\to -q_3)$ is the only conserved symmetry. The position of the coordinate origin is defined by fixing parameters α and $\beta = 1-\alpha$ and can be taken at will because the two solutions differing by the shift of the origin along the internuclear axis are related to each other by an unessential coordinate-dependent phase factor [14].

We note that, for simplicity, we call the operator defined in Eq. (6) "Hamiltonian" although its eigenvalues have the dimensionality of (length)$^2\times$ energy. The dimensionality of $\omega = \rho v$ is (length)^2/time. It is tempting to say that the parameter ω is "frequencylike" because of the form of the last two terms in Eq. (6). In the SI system, these two terms read as $\omega L_3 + m_e\omega^2 q^2/2$ and have the dimensionality (length)$^2\times$ energy just like the eigenvalues of the transformed Hamiltonian (6). Finally, the timelike variable τ with dimensionality time/(length)^2 (reciprocal to that of ω) has been introduced in order to obtain the right-hand side of Eq. (5) in the form of the standard time-dependent Schrödinger equation.

For slow collisions, when an adiabatic approach is appropriate, we look for the solutions of Eq. (5) in the form of an expansion

$$f(\mathbf{q},\tau) = \sum_j g_j(\tau)\Phi_j(\mathbf{q},R(\tau),\omega)\exp\left(-i\int_0^\tau E_j(R(\tau'),\omega)d\tau'\right) \tag{8}$$

in terms of the eigenfunctions $\Phi_j(\mathbf{q},R(\tau),\omega)$ of the instantaneous Hamiltonian $H(\tau)\equiv H(R,\omega)$ defined in Eq. (6):

$$H(R,\omega)\Phi_j(\mathbf{q},R,\omega) = E_j(R,\omega)\Phi_j(\mathbf{q},R,\omega), \tag{9}$$

where for the purposes of this work, we have suppressed the τ dependence of R but made explicit the parametric dependence of all quantities on ω. We call the complete set of eigenfunctions $\Phi_j(\mathbf{q},R,\omega)$ *dynamical adiabatic states* (DAS) and the eigenvalues $E_j(R,\omega)$ DAPEC because in addition to internuclear separation R, they also depend on dynamic parameter $\omega = \rho v$. For $\omega\neq 0$, due to the presence of the harmonic oscillator potential in Eq. (6), the spectrum of the Hamiltonian $H(R,\omega)$ is discrete. The general properties of the DAPEC for the complete range of real internuclear separations R, from 0 to $+\infty$, have been studied in our previous work [9].

Here, we are interested in analytic continuations of DAPEC into the complex R plane, that is, the solutions of the eigenvalue problem (9) for complex values of R. This will enable us to detect the various branch points $R_b(i,f,\omega)$ connecting the pairs of the complex DAPEC $E_i(R,\omega)$ and $E_f(R,\omega)$ and eventually use them in calculations of the single-pass electron transition probabilities, given by an expression analogous to Eq. (1):

$$p_{if}(\rho,v) = \exp\left(-\frac{2}{\hbar}\mathrm{Im}\int_L E(R,\omega)\frac{dR}{\tilde{v}_R(R,\rho,v)}\right), \tag{10}$$

where the generalized radial velocity is related to the standard radial velocity through the relation $\tilde{v}_R(R,\rho,v) = dR/d\tau = v_R(R,\rho,v)R^2$. In our case, the straight-line ionic trajectories $v_R(R,\rho,v) = v(1-\rho^2/R^2)^{1/2}$. The definitions of the contour L and the multivalued complex function $E(R,\omega)$ in Eq. (10) are analogous to those given in connection with Eq. (1). We note that, as can be seen from Eqs. (6) and (9), in the case $\omega = 0$ any DAPEC $E_j(R,0)$ is related to the usual PEC $\varepsilon_j(R)$ of the two-Coulomb-center problem by the relation

$$E_j(R,0) = \varepsilon_j(R)R^2, \tag{11}$$

so that in this limit Eq. (10) reduces to Eq. (1).

We also note that the given classical trajectory is not determined only by $\omega = \rho v$, but rather by ρ and v separately, for example, $R^2 = \rho^2 + v^2t^2$. The two collisions characterized by the same $\omega = \rho v$, but different ρ and v do not lead to the same transition probabilities. This is explicitly seen in Eq. (10) where $E(R,\omega)$ indeed depends only on ω, but the radial velocity $v_R = v(1-\rho^2/R^2)^{1/2}$ depends separately on ρ and v. [Another way to conclude the same is to start from the fact that quantum dynamics is determined by the τ dependence of the Hamiltonian $H(\tau)$. Although the last two terms in Eq. (6) depend only on ω, the internuclear separation $R(\tau) = \rho/\cos(\omega\tau)$ depends separately on ρ and v.]

III. METHOD OF CALCULATION

In order to solve the (complex) eigenvalue problem (9) when R is a complex number, we use the same method as

in our previous work [9] related to the investigation of the dynamical adiabatic eigenvalues for real values of R. A matrix representation of the Hamiltonian is constructed by using the prolate spheroidal coordinates (ξ,η,ϕ) of the electron, the direct product of Lagrange-mesh bases [15,16], to represent (ξ,η) degrees of freedom and a standard sine and cosine basis for azimuthal angle ϕ. In this representation, the symmetry blocks, corresponding to states with $\pi_3 = \pm 1$, are decoupled and explicit expressions for matrix elements of all operators are given in Ref. [9]. Complex eigenvalues are obtained by diagonalization of the Hamiltonian matrix and convergence of the results is controlled by increasing the number of basis functions.

In all our calculations we start with the eigenvalues obtained on the real R axis for particular initial $R_i = (\mathrm{Re}R_i, 0)$ and order them according to $E_1 < E_2 < E_3 < \ldots$. Then, the eigenvalues are analytically continued into the complex R plane along the straight line parallel to the ImR axis connecting R_i and $R_f = (\mathrm{Re}R_i, \mathrm{Im}R_f)$. In order to keep track of the complex eigenvalues $E_1, E_2, E_3, \ldots$, the steps of advancing into the complex plane along this straight line have to be small. In that case, at each step, it is possible to assign the index j to the eigenvalue which is closest to the E_j calculated in the previous step. Alternatively, one can use a three-step extrapolation scheme to determine accurate predictions of eigenvalues in the forthcoming step and in such a way increase the steps for advancing into the complex plane. Repeating this procedure for a range of initial R_i's one can obtain the complex surfaces $E_j(R,\omega)$, $j = 1,2,3,\ldots$, in the certain domain of the complex R plane. If there is a branch point $R_b(j,j';\omega)$ connecting the eigenvalues $E_j(R,\omega)$ and $E_{j'}(R,\omega)$, the graphs of surfaces $\mathrm{Re}E_j(R,\omega)$, $\mathrm{Im}E_j(R,\omega)$, $\mathrm{Re}E_{j'}(R,\omega)$, and $\mathrm{Im}E_{j'}(R,\omega)$ will appear with the discontinuities along the "cuts" in the line parallel to the ImR axis connecting the $R_b(j,j';\omega)$ and $(\mathrm{Re}R_b, +\infty)$.

In order to precisely locate various branch points, we have developed a searching algorithm which relies on the fact that close enough to the branch point the two eigenvalues are represented with

$$E_{j,j'}(R,\omega) = a \pm b\sqrt{R - R_b(j,j';\omega)}. \tag{12}$$

Assuming that we have two initial guesses for the branch point, R_1 and R_2, the branch point is obtained from Eq. (12) as

$$R_b(j,j';\omega) = \frac{R_1[E_j(R_2) - E_{j'}(R_2)]^2 - R_2[E_j(R_1) - E_{j'}(R_1)]^2}{[E_j(R_2) - E_{j'}(R_2)]^2 - [E_j(R_1) - E_{j'}(R_1)]^2}. \tag{13}$$

The iteration process consists in taking as new guesses $R_1 = R_2$ and $R_2 = R_b(j,j';\omega)$ and repeating the procedure until the required convergence is achieved.

IV. RESULTS AND DISCUSSION

We present here the results for a generic asymmetric system, defined with $Z_A = 1$ and $Z_B = 2$, that is for the HeH^{2+} quasimolecular system. In order to investigate some of the inelastic, that is, excitation or charge-exchange processes in collisions of $H^+ + He^+(1s$ or $2s,2p)$ or $H(1s) + He^{2+}$, it is necessary to study the distribution (and the ω dependence) of the branch points connecting the low-lying DAPEC.

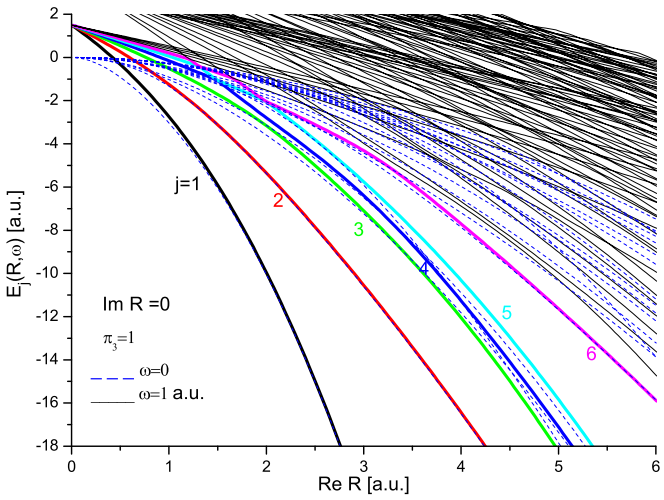

FIG. 1. (Color online) The 90 lowest eigenvalues (DAPEC) for symmetric ($\pi_3 = 1$) states of the $(HeH)^{2+}$ collision system ($Z_A = 1, Z_B = 2$) as functions of the internuclear separation R at real R axis [$\mathrm{Im}(R) = 0$] for $\omega = 1$ a.u. (solid curves) and the lowest 20 DAPEC for $\omega = 0$ [dashed (blue) curves].

The solid curves in Fig. 1 show the R dependence on the real R axis [$\mathrm{Im}(R) = 0$] of the 90 lowest symmetric ($\pi_3 = 1$) eigenvalues $E_j(R,\omega)$ for $\omega = 1$. As a dominant structure, one can notice the overlapping manifolds of the DAPEC which start at $R = 0$ from the points of high degeneracy corresponding to oscillatorlike energies

$$E_j(0,\omega) = (N + 3/2)\omega, \quad N = 0,2,4,\ldots \tag{14}$$

and then spreading toward larger distances where they all tend toward large negative values. The general properties of the DAPEC on the real R axis, including the limiting cases $R \to 0$ and $R \to \infty$, are discussed in detail in Ref. [9]. In Fig. 1, the lowest six DAPEC are labeled with $j = 1$–6 and in the following, we shall mainly concentrate on the analytic properties of these eigenvalues as they are analytically continued into the complex R plane. That is, we shall study the distribution and ω dependence of branch points connected the pairs of these eigenvalues.

The dashed (blue) curves in Fig. 1 are the 20 lowest symmetric DAPEC for $\omega = 0$. They are related to the usual PEC $\varepsilon_j(R)$ of the HeH^{2+} molecular ion by the relation (11). One can notice that the dashed (blue) and solid curves merge as $R \to \infty$.

As is shown in Ref. [9], a similar dominant structure of the DAPEC is also found for antisymmetric ($\pi_3 = -1$) states. The only difference is that degenerate manifolds at $R = 0$, which are again given by Eq. (14), now correspond to $N = 1,3,5,\ldots$. In the rest of the article, we shall concentrate on $\pi_3 = 1$ states without specifically pointing this out.

Due to the relationship (11) and the fact that $E(R,\omega)$ and $E(R,0)$ merge as $R \to \infty$, it is more convenient to consider the case of intermediate and large real internuclear separations by studying the R dependence of the scaled DAPEC, $E_j(R,\omega)/R^2$, because these quantities should asymptotically approach the atomic levels of separated atoms. However, due to the well-known increase of the density of excited states in

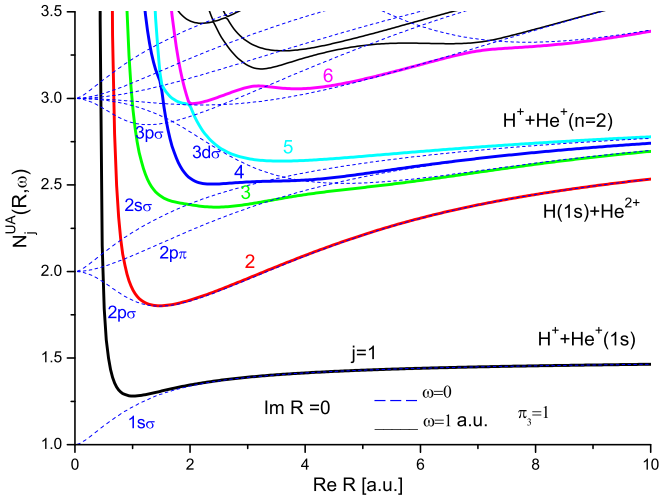

FIG. 2. (Color online) Segment of low-lying scaled DAPEC represented in terms of "effective united-atom principal quantum number" [Eq. (15)] (solid curves). Also shown [dashed (blue) curves] are the standard PEC of the $(HeH)^{2+}$ molecular ion labeled by united-atom quantum numbers.

Coulombic systems, it is even more convenient for graphical representation to use the "effective united-atom principal quantum number"

$$N_j^{\rm UA}(R,\omega) = (Z_A + Z_B)[-2E_j(R,\omega)/R^2]^{-1/2}. \qquad (15)$$

This quantity has a property that $N_j^{\rm UA}(0,0) = (Z_A + Z_B)[-2\varepsilon_j(0)]^{-1/2} = 1,2,3,\ldots$ is the united-atom principal quantum number of the HeH^{2+} system. In Fig. 2, the R dependence of $N_j^{\rm UA}(R,\omega)$ is shown for the fragment of the low-lying DAPEC (solid curves) and PEC [dashed (blue) curves] which correspond to those shown in Fig. 1. Both sets of curves, corresponding to DAPEC and PEC, asymptotically (as $R \to \infty$) approach the same values corresponding to the unperturbed atomic levels, although there are some differences in asymptotic behavior, which are not visible in these figures and are discussed in Ref. [9]. In any case, this representation is useful in predicting which DAPEC are important and should be included when describing various inelastic processes.

In our investigations, we shall start from the known set of branch points for $\omega = 0$ corresponding to PEC of the HeH^{2+} system [17] and then study the behavior of some representative examples of these branch points when ω is systematically increased. In addition, the exact crossings of PEC corresponding to rotational couplings will generate additional branch points of the DAPEC for $\omega \neq 0$ which we call L_3 branch points. Each following subsection is entitled by two sets of united-atom quantum numbers of the PEC that are connected by a branch point at $\omega = 0$.

A. Hidden crossing between the $1s\sigma$ and $2p\sigma$ surfaces

We start with the ω dependence of the branch-point position connecting the ground and the first excited DAPEC, labeled $j = 1$ and 2 in Figs. 1 and 2. The position of the branch point at $\omega = 0$, connecting the $1s\sigma$ and the $2p\sigma$ complex PEC is known to be at $R_b(1,2;\omega = 0) = (1.213,1.364)$ [17]. With our search method we have easily confirmed this result. Figure 3 shows how real and imaginary parts of the complex DAPEC $E_1(R,0)$ and $E_2(R,0)$ look when they are analytically continued from the real axis ($\mathrm{Im}R = 0$) towards the increasing values of $\mathrm{Im}R$ along the straight lines $\mathrm{Re}R =$constant in the complex R plane. The points on the surfaces that correspond to the position of the branch point are labeled by somewhat exaggerated spherical symbols. The pairs of functions $\{\mathrm{Re}E_1,\mathrm{Re}E_2\}$ and $\{\mathrm{Im}E_1,\mathrm{Im}E_2\}$ can be "pasted" along the cuts $\{\mathrm{Re}R = \mathrm{Re}R_b,\ \mathrm{Im}R \in (\mathrm{Im}R_b, +\infty)\}$ to obtain the multivalued analytic function of which E_1 and E_2 are single-valued branches.

In the two-Coulomb-center problem, this branch point is actually the first member (closest to the real R axis) of the so-called $Q_{000}^{(2)}$ series which connects the $1s\sigma$ surface with a series of other surfaces [17]. [Here, $Q_{n_1n_2m}^{(i)}$ stands for the separated-atom parabolic quantum numbers $(n_1n_2m) = (000)$ of the $1s\sigma$ state which is asymptotically localized on center $i = 2$, i.e., He^{2+}.] For brevity, we shall refer to branch points originating from this one for $\omega \geqslant 0$ as Q_2 branch points.

Starting from $R_b(1,2;\omega = 0)$ one can, by adding small increments to ω, construct the trajectory of $R_b(1,2;\omega)$ in the complex R plane, as shown in Fig. 4. It can be seen, however, that for some $\omega \in (0.75,0.8)$, the $R_b(1,2;\omega)$ turns over into $R_b(1,5;\omega)$, that is, it connects the surfaces labeled 1 and 5 (not 2). In order to understand the cause of this phenomenon, we investigate in the next subsection the trajectory of another branch point related to eigenvalue 2, namely, the one which at small values of ω connect surfaces 2 and 3.

B. $2p\sigma - 2p\pi$ and $2s\sigma - 2p\pi$ rotational couplings in the united-atom limit

At $\omega = 0$, the eigenvalues labeled 2 and 3 correspond to $2p\sigma$ and $2p\pi$ PEC shown as dashed lines in Fig. 2 which are degenerate at $R = 0$. As is shown in Fig. 5 when ω increases from zero, the L_3 branch point $R_b(2,3;\omega)$ arises and at first retains its character, but then is transformed into $R_b(2,4;\omega)$ somewhere in the interval $\omega \in (0.3,0.5)$ and subsequently into $R_b(2,5;\omega)$ somewhere in the interval $\omega \in (0.75,0.8)$. The last interval is exactly the same as the one mentioned in the preceding subsection where the transformation of the Q_2 branch point from $R_b(1,2;\omega)$ to $R_b(1,5;\omega)$ occurs, so it is the interval where the redistribution of branch points between surfaces 1, 2, and 5 occurs. This is confirmed in Fig. 6 where the structure of surfaces 1, 2, and 5 in the vicinity of branch points $R_b(1,5;\omega = 0.8)$ and $R_b(2,5;\omega = 0.8)$ is shown. It can be seen that indeed there is no direct connection (branch point) between surfaces 1 and 2, but rather surface 5 is connected with both of them.

Another example of the same kind of redistribution of the branch points is the above-mentioned transformation of the L_3 branch point $R_b(2,3;\omega)$ into $R_b(2,4;\omega)$ somewhere in the interval $\omega \in (0.3,0.5)$. It can be explained by the trajectory of another L_3 branch point $R_b(3,4;\omega)$, part of which is also shown in Fig. 5. At $\omega \to 0$, it corresponds to $2s\sigma - 2p\pi$ rotational coupling at small R. It can be seen from Fig. 5 that $\mathrm{Re}R_b(3,4;0.3) < \mathrm{Re}R_b(2,3;0.3)$ while $\mathrm{Re}R_b(3,4;0.5) > \mathrm{Re}R_b(2,4;0.5)$. It means that there exists some critical $\omega_c \in (0.3,0.5)$ such that $\mathrm{Re}R_b(3,4;\omega_c) = \mathrm{Re}R_b(2,3;\omega_c - \epsilon)$

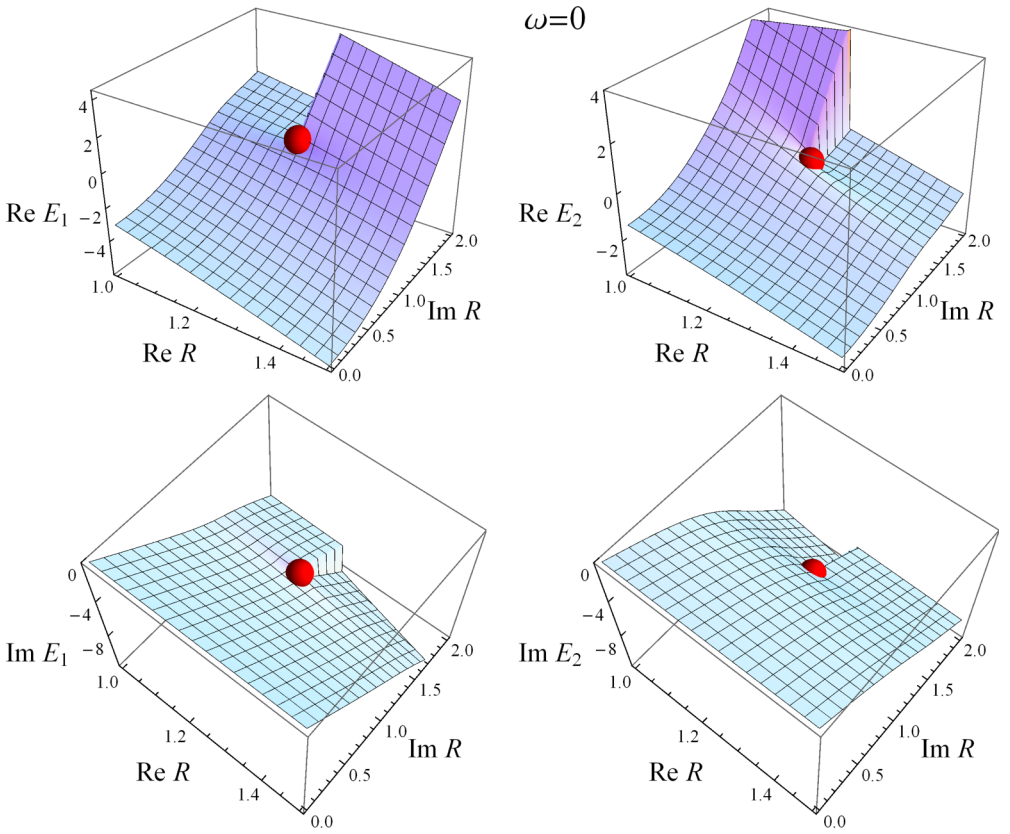

FIG. 3. (Color online) Analytic continuations of $E_1(R,\omega=0)$ and $E_2(R,\omega=0)$ from the real R axis into the complex R plane along the paths: ReR = const. The (exaggerated) spherical symbols are points on the surfaces corresponding to branch point $R_b(1,2;\omega=0)$. All quantities are in atomic units.

$=\mathrm{Re}R_b(2,4;\omega_c+\epsilon)$, $\mathrm{Im}R_b(3,4;\omega_c) < \mathrm{Im}R_b(2,3;\omega_c-\epsilon) = \mathrm{Im}R_b(2,4;\omega_c+\epsilon)$, $(\epsilon\to 0+)$, so that $R_b(2,3;\omega)\to R_b(2,4;\omega)$ at $\omega=\omega_c$.

Based on the last example, we can formulate the general conditions for occurrence of the transformation of a branch point $R_b(j,j';\omega_c)\to R_b(j,j'';\omega_c)$ at $\omega_c\in(\omega_1,\omega_2)$ due to the

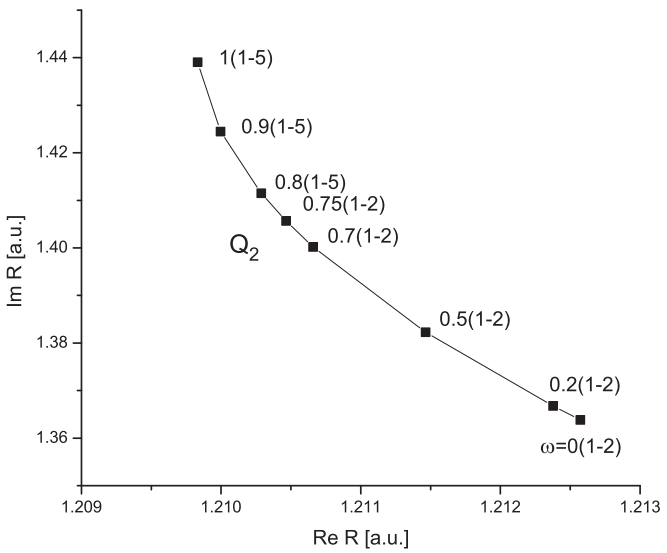

FIG. 4. Trajectory of the branch point Q_2 which starts as $R_b(1,2;\omega)$ for $\omega\in(0,0.75)$ but transforms into $R_b(1,5;\omega)$ in the interval $\omega\in(0.75,0.8)$. In all figures, branch points $R_b(j,j';\omega)$ are labeled as $\omega(j-j')$.

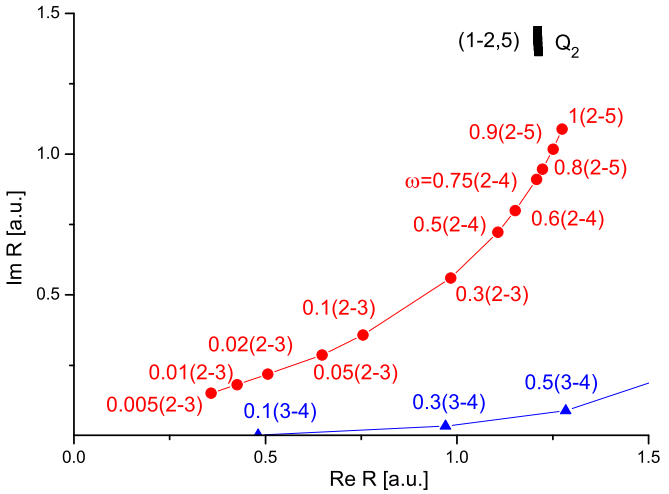

FIG. 5. (Color online) Full circles represent the trajectory of the L_3 branch point which starts as $R_b(2,3;\omega)$ for $\omega\in(0,0.3)$, transforms into $R_b(2,4;\omega)$ in the interval $\omega\in(0.3,0.5)$, and into $R_b(2,5;\omega)$ in the interval $\omega\in(0.75,0.8)$. Full triangles are part of the trajectory of another L_3 branch point $R_b(3,4;\omega)$. Full squares labeled (1-2,5) are the replica of the Q_2 branch points from Fig. 4.

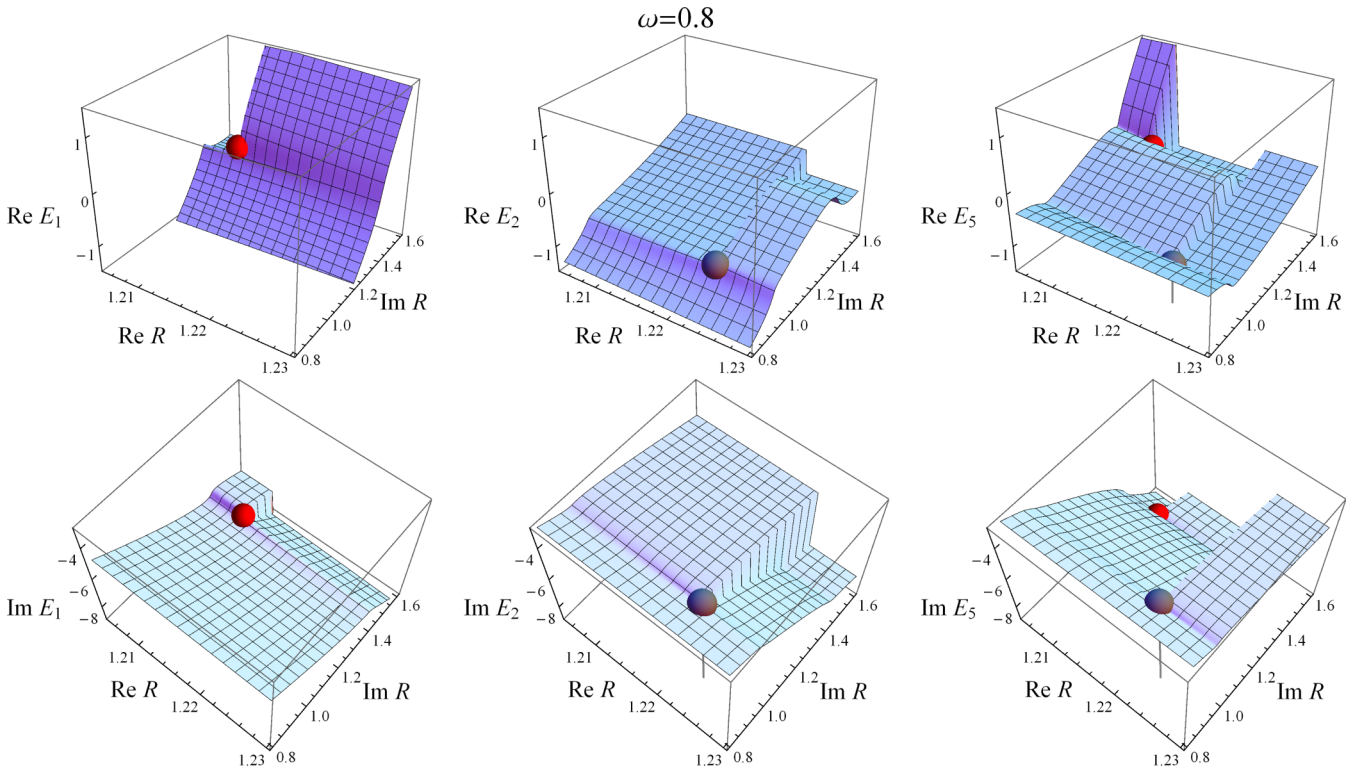

FIG. 6. (Color online) Analytic continuations of $E_1(R,\omega = 0.8)$, $E_2(R,\omega = 0.8)$, and $E_5(R,\omega = 0.8)$ from the real R axis into the complex R plane along the paths: ReR = const. The spherical symbols are points on the surfaces corresponding to branch points: in the first column $R_b(1,5;\omega = 0.8)$, in the second column $R_b(2,5;\omega = 0.8)$, and in the third column $R_b(1,5;\omega = 0.8)$ and $R_b(2,5;\omega = 0.8)$. All quantities are in atomic units.

existence of the branch point $R_b(j',j'';\omega)$:

$$\begin{aligned} &\mathrm{Re}R_b(j',j'';\omega_1) < \mathrm{Re}R_b(j,j';\omega_1),\\ &\mathrm{Re}R_b(j',j'';\omega_2) > \mathrm{Re}R_b(j,j'';\omega_2),\\ &\mathrm{Im}R_b(j',j'';\omega_1) < \mathrm{Im}R_b(j,j';\omega_1),\\ &\mathrm{Im}R_b(j',j'';\omega_2) < \mathrm{Im}R_b(j,j'';\omega_2). \end{aligned} \tag{16}$$

As we shall see in the following subsections, such transformations are frequent, especially at small values of ReR.

C. Rotational coupling between the $3d\sigma$ and $2p\pi$ states

First, we complete the trajectory of the L_3 branch point $R_b(3,4;\omega)$ of the preceding subsection for the range $\omega \in (0.1,2)$. These results are shown in Fig. 7 and labeled (3-4). However, there is another family of L_3 branch points connecting DAPEC 3 and 4. Namely, the exact crossing in Fig. 2 between the $3d\sigma$ and $2p\pi$ PEC, which in standard adiabatic representation indicates a region of strong rotational coupling, appears as an avoided crossing between two DAPEC labeled 3 and 4. Starting from the exact crossing $R'_b(3,4;\omega = 0) = (4.507,0)$ we have calculated the trajectory of $R'_b(3,4;\omega)$, which is shown in Fig. 7 and labeled (3-4)$'$. Unlike the Q_2 branch points connecting (1-2,5) and L_3 branch points connecting (2-3,4,5) (which are replicated in Fig. 7 from Figs. 4 and 5), neither (3-4) nor (3-4)$'$ L_3-branch points undergo the transformations of the kind described by Eqs. (16).

D. $2p\sigma - 3p\sigma$ member of the $S_{p\sigma}$ series of branch points

In the two-Coulomb-center problem, one finds the S_{lm} series of branch points [8,10]. Each series consists of an

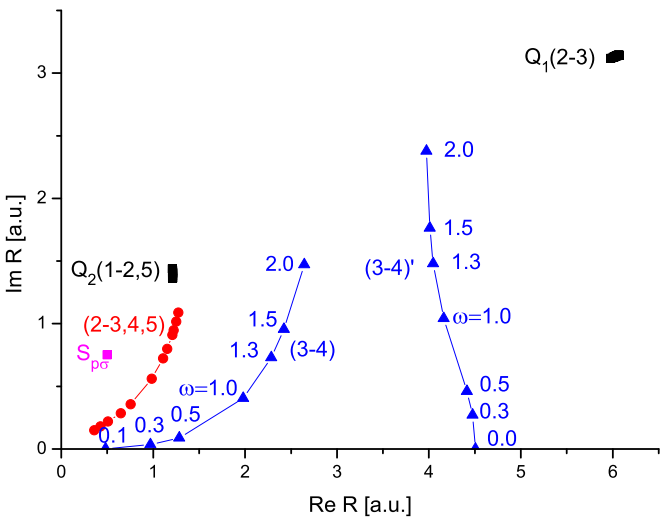

FIG. 7. (Color online) Full triangles labeled (3-4) correspond to L_3 branch points originating from $2s\sigma - 2p\pi$ rotational coupling in the united-atom limit at $\omega = 0$. Full triangles labeled (3-4)$'$ correspond to L_3 branch points originating from $3d\sigma - 2p\pi$ exact crossing at $\omega = 0$. Full squares labeled Q_2(1-2,5) are the replica of Fig. 4 and full circles labeled (2-3,4,5) are the replica of Fig. 5. Also shown are the positions of $S_{p\sigma}$ series and Q_1 branch points.

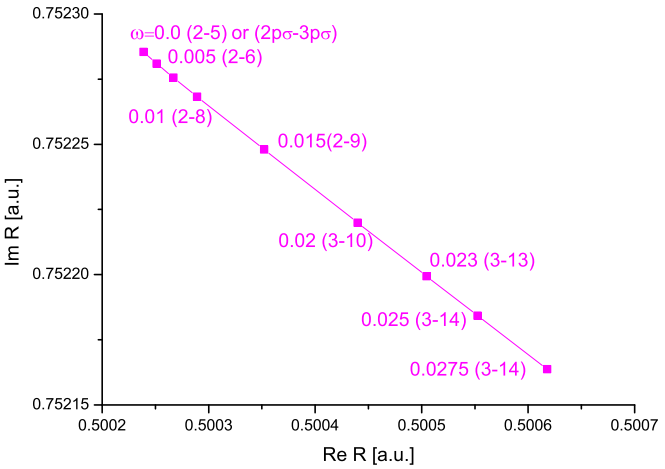

FIG. 8. (Color online) Trajectory of the branch point which starts as the first member of $S_{p\sigma}$ series $R_b(2,5;0)$ but after a series of transformations ends up as $R_b(3,14;0.0275)$.

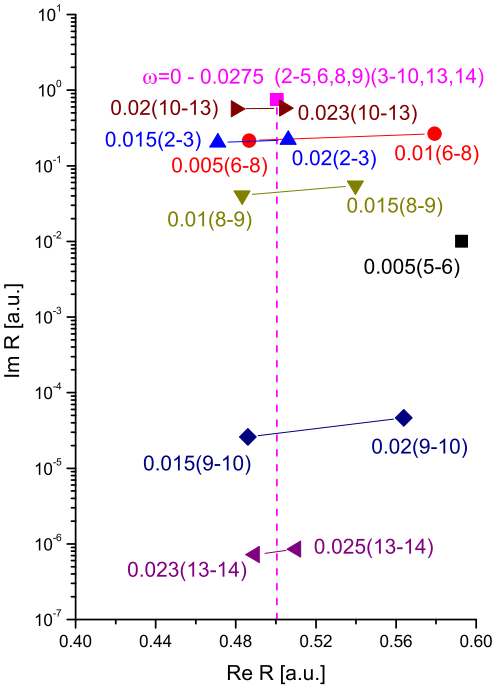

FIG. 9. (Color online) Positions of the various pairs of branch points responsible for the transformations along the trajectory shown in Fig. 8. This trajectory is here contained within the uppermost square symbol.

infinite set of branch points $R_b(Nlm)$ connecting pairwise PEC $\varepsilon_{Nlm}(R) - \varepsilon_{N+1lm}(R)$ consecutively for all $N \geqslant l+1$. All branch points of a series are localized within the small domain of the complex R plane and as $N \to \infty$ approach a limiting point $R_b(\infty lm)$. Transitions caused by these series of branch points are responsible for the promotion of the electron into the continuum in slow collisions, that is, they explain the mechanism of the ionization process [8,10,17].

As an example, we consider the $S_{p\sigma}$ series of the HeH^{2+} system, whose approximate location is shown in Fig. 7. We shall explore how the first member of this series connecting $2p\sigma - 3p\sigma$ PEC, namely, $R_b(210)$ or in our notation $R_b(j=2,j'=5;\omega=0) = (0.500\,239, 0.752\,285)$, transforms for $\omega \neq 0$. We note that the second member of the $S_{p\sigma}$ series, connecting $3p\sigma - 4p\sigma$ PEC, is located at $R_b(310) \equiv R_b(5,11;0) = (0.490\,825, 0.720\,151)$, very close to the first member.

Figure 8 shows the trajectory of branch points for $\omega \in (0, 0.0275)$ which originate from $R_b(2,5;\omega=0)$. It can be seen that even for this small interval of ω the branch points undergo a series of transformations. All of the indicated changes in the labels of surfaces that are connected by a particular branch point can be explained by the fulfillment of conditions (16) as is documented in Fig. 9.

Note first that on the scale of Fig. 9, all branch points from Fig. 8 are localized within the uppermost square symbol, so that their real parts $\mathrm{Re}R_b(j,j';\omega)$ are approximately defined by the dashed vertical line. Then, in order for the transformation $R_b(j,j';\omega_1) \to R_b(j,j'';\omega_2)$ to occur, the first two conditions from Eq. (16) simply mean that the line connecting branch points $R_b(j',j'';\omega_1)$ and $R_b(j',j'';\omega_2)$ in Fig. 9 should cross the vertical dashed line. The second two conditions from Eq. (16) simply mean that all branch points $R_b(j',j'';\omega)$ should lie below the uppermost square in Fig. 9, as they do.

The first transformation in Fig. 8, $R_b(2,5;0) \to R_b(2,6;0.005)$, occurs because $R_b(5,6;0) = (0,0)$ (not shown) in Fig. 9 is on the left of the vertical dashed line and $R_b(5,6;0.005)$ [shown in Fig. 9 as 0.005(5-6)] is on the right. The next two transformations $R_b(2,6;0.005) \to R_b(2,8;0.01) \to R_b(2,9;0.015)$ occur because, as seen from Fig. 9, the lines connecting branch points $R_b(6,8;0.005) - R_b(6,8;0.01)$ and $R_b(8,9;0.01) - R_b(8,9;0.015)$ both cross the vertical dashed line. In further transformation $R_b(2,9;0.015) \to R_b(3,10;0.02)$ both indices are changed, and this is explained by the fact that in Fig. 9 the lines connecting $R_b(2,3;0.015) - R_b(2,3;0.02)$ and $R_b(9,10;0.015) - R_b(9,10;0.02)$ both cross the vertical dashed line. The next two transformations $R_b(3,10;0.02) \to R_b(3,13;0.023) \to R_b(3,14;0.025)$ occur because, as seen from Fig. 9, the lines connecting branch points $R_b(10,13;0.02) - R_b(10,13;0.023)$ and $R_b(13,14;0.023) - R_b(13,14;0.015)$ both cross the vertical dashed line. The last branch point shown in Fig. 8, $R_b(3,10;0.0275)$, is reached without any transformation.

We have found difficulties in extending the calculations to values of $\omega > 0.0275$. The reason is probably the fact that still higher states are involved in transformations. In any case, the conclusion is that this member of the $S_{p,\sigma}$ series, and presumably the other members, with the increase of ω still stay within the limited domain of the complex R plane and are related to complicated connections with highly excited states. Basically, in this way it seems that the essential role of the S series in promoting electron into highly excited (and eventually ionized) states is retained in dynamical adiabatic theory.

E. Hidden crossing between the $2p\sigma$ and $3d\sigma$ surfaces

The last example considers the hidden crossings located at relatively large $\mathrm{Re}R$ which originate at $\omega = 0$ from the first member of the $Q^{(1)}_{000}$ series [17], namely, $R_b(2,3;0) = (6.067, 3.145)$ which connects PEC $2p\sigma$ and $3d\sigma$. Accordingly, we shall refer to these branch points $R_b(2,3;\omega)$ as to

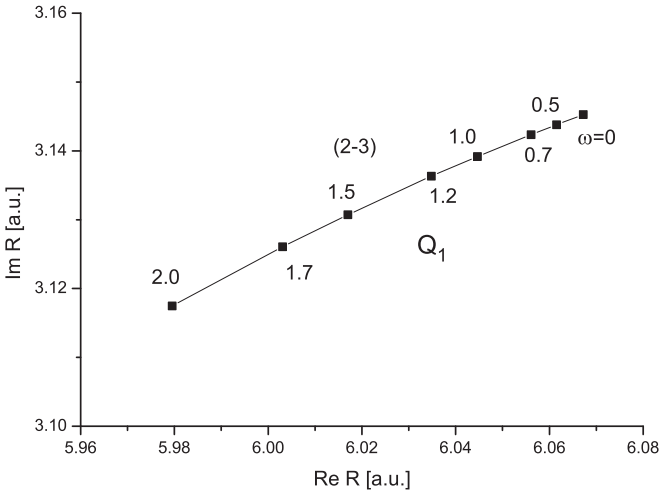

FIG. 10. Trajectory of the Q_1 branch points $R_b(2,3;\omega)$ for $\omega \in (0,2)$ which starts at $\omega = 0$ connecting the $2p\sigma$ and $3d\sigma$ PEC.

Q_1 branch points. As can be seen from Fig. 10, for $\omega \in (0,2)$ the Q_1 branch points stay within the small region of the complex R plane and there are no changes of indices of surfaces that are connected. The relative position of the location of the Q_1 branch points with respect to other branch points studied is shown in Fig. 7.

V. CONCLUDING REMARKS

In general, we can conclude that the hidden crossings (such as Q_1 and Q_2) involving a change of parameter ω occupy relatively small regions in the complex R plane. On the other hand, the L_3 crossings extend over the regions with considerable changes of both ReR and ImR, as is seen from Fig. 7. This "motion" of the L_3 crossings leads to appearance of a phenomenon in the dynamical adiabatic basis, namely, the possibility of change of the indices of eigenvalues that are connected by the branch points which lie further away in the complex plane and that are "overtaken" by some moving L_3 branch points. This has consequences on the way how the probabilities of various inelastic transitions are to be calculated.

For example, as is already discussed with connection to Fig. 5, with the increase of ω, the L_3 branch point between the third and fourth states moves from $R = 0$ to the right and at some $\omega_c \in (0.3,0.5)$ overtakes the upper L_3 branch point between the second and third states. For $\omega > \omega_c$, the upper branch point connects the second and fourth states. With further increase of ω, a branch point between the fourth and fifth states (not shown in Fig. 5) overtakes the upper L_3 branch point and changes again its connection from the second and fourth to second and fifth states. At particular $\omega_{Q2} \in (0.75,0.8)$, the upper L_3 branch point passes under the Q_2 branch point and changes its connection from the first and second to the first and fifth states. Therefore, when calculating the charge-exchange cross section from the ground state of He^+ to the ground state of the hydrogen atom, the expression for transition probability $(1 \to 2)$ as a function of the impact parameter ρ alters from

$$P_{\text{ch-ex}} = 2p_{Q2}(1-p_{Q2})\big(1-p_L+p_L^2\big)(1-p_{Q1}) \qquad (17)$$

at $\rho < \omega_{Q2}/v$ to

$$P_{\text{ch-ex}} = 2p_{Q2}(1-p_{Q2})p_L(1-p_{Q1}) \qquad (18)$$

at $\rho > \omega_{Q2}/v$, where p_{Q2}, p_L, and p_{Q1} are elementary single-pass transition probabilities due to Q_2, upper L_3, and Q_1 branch points, respectively.

This rearrangement of couplings cannot be explained so easily as the hidden and avoided crossings in the separable two-Coulomb-center problem. All L_3 crossings originate from exact crossings of the PEC of *different symmetry* in this problem which have accidental distribution on the R axis. The additional operator $\Lambda(\mathbf{q}) = \omega L_3 + \frac{1}{2}\omega^2 q^2$ in dynamical representation (6) is not the standard potential. On the one hand, it is covariant with respect to translation along the $\mathbf{R}$ axis like a constant. On the other hand, each term in $\Lambda(\mathbf{q})$ has a very pronounced position. Both terms, being of completely different nature (first is a differential operator and second is a standard function), compensate each other in the leading order, and a separate analysis of their role is meaningless. At the same time, $\Lambda(\mathbf{q})$ destroys separability and existence of the one-dimensional effective potentials.

As a final remark, we note that the narrow avoided crossings, mentioned in the Introduction, are absent in the HeH^{2+} system (they appear for higher values of Z_B/Z_A). As they originate from underbarrier electronic exchange and are not directly related to the rotation of the internuclear axes, we expect that they will show a weak ω dependance similarly to that of the hidden crossings.

ACKNOWLEDGMENTS

This work was partly supported by Serbia-JINR collaboration program. T.P.G. acknowledges the support by the Ministry of Education, Science and Technological Development of the Republic of Serbia through the Project No. 171020. We are indebted to R. McCarroll for critical reading of the manuscript.

[1] R. McCarroll and D. S. F. Crothers, Adv. At. Mol. Opt. Phys. **32**, 253 (1994).
[2] J. Macek, J. Phys. B: At. Mol. Phys. **1**, 831 (1968).
[3] C.-N. Liu, A.-T. Le, T. Morishita, B. D. Esry, and C. D. Lin, Phys. Rev. A **67**, 052705 (2003).
[4] E. A. Solov'ev, Theor. Math. Phys. **28**, 757 (1976).
[5] V. V. Serov, V. L. Derbov, B. B. Joulakian, and S. I. Vinitsky, Phys. Rev. A **75**, 012715 (2007).
[6] E. Y. Sidky and B. D. Esry, Phys. Rev. Lett. **85**, 5086 (2000).
[7] A. Hamido, J. Eiglsperger, J. Madronero, F. Mota-Furtado, P. O'Mahony, A. L. Frapiccini, and B. Piraux, Phys. Rev. A **84**, 013422 (2011).
[8] E. A. Solov'ev, Sov. Phys.–Usp. **32**, 228 (1989).
[9] T. P. Grozdanov and E. A. Solov'ev, Phys. Rev. A **88**, 022707 (2013).
[10] E. A. Solov'ev, J. Phys. B: At. Mol. Opt. Phys. **38**, R153 (2005).

[11] C. Zener, Proc. R. Soc. **137**, 696 (1932).
[12] T. P. Grozdanov and E. A. Solov'ev, J. Phys. B: At. Mol. Phys. **15**, 3871 (1982).
[13] T. P. Grozdanov and E. A. Solov'ev, Phys. Rev. A **44**, 5605 (1991).
[14] T. P. Grozdanov and E. A. Solov'ev, Eur. Phys. J. D **6**, 13 (1999).
[15] M. Vincke and D. Baye, J. Phys. B: At. Mol. Opt. Phys. **39**, 2605 (2006).
[16] D. Baye, A. J. de ter Beerst, and J.-M. Sparenberg, J. Phys. B: At. Mol. Opt. Phys. **42**, 225102 (2009).
[17] T. P. Grozdanov and E. A. Solov'ev, Phys. Rev. A **42**, 2703 (1990).